

# An Energy Storage Principle using Bipolar Porous Polymeric Frameworks\*\*

Ken Sakaushi,\* Georg Nickerl, Florian M. Wisser, Daisuke Nishio-Hamane, Eiji Hosono, Haoshen Zhou,\* Stefan Kaskel, and Jürgen Eckert

Our society has a great demand for highly efficient and mobile energy storage,<sup>[1–6]</sup> which furthermore has to be sustainable from an economic and environmental point of view. For instance, the batteries for automotive applications require a super-high specific energy that is comparable to the conventional internal combustion engines.<sup>[7]</sup> Much effort has been focused on finding the proper balance between power and energy of electrical energy storage devices,<sup>[8–12]</sup> which, at the same time, combine the rate performance of super-capacitors with the typical specific energy of batteries. The aim is to develop an energy storage principle that can deliver a 2–3 times higher specific energy than current batteries with a high rate capability.

Herein, we demonstrate that amorphous covalent triazine-based frameworks (ACTFs) can be successfully used as a cathode material. These frameworks undergo a unique Faradaic reaction, as they can be present in a p-doped and an n-doped state. During charging and discharging, the polymeric cathode changes its charge state through a continuous, linear bipolar redox mechanism. The outcome is a remarkably high specific energy of 1084 Wh kg<sup>−1</sup> combined with a high specific power of 13238 W kg<sup>−1</sup> based on the mass of the framework. The present finding could mark a new route to improve the performance of lithium-based energy storage devices by employing artificial porous polymeric frameworks as electrode materials.

Lithium batteries based on the intercalation mechanism seem to have reached the physical limit of specific energy owing to the low capacity of the known cathode materials.<sup>[1,3,5,7]</sup> In contrast, rechargeable lithium–air batteries,<sup>[13]</sup> which can deliver theoretically super-high specific energy, generally suffer from a poor power performance because of the low diffusion rate of O<sub>2</sub> within the porous catalytic electrodes.

Porous polymeric frameworks are synthesized from the rational assembly of organic monomers.<sup>[14–18]</sup> Their properties are tunable by choosing various combination of monomers to create artificial purely organic frameworks with a high potential for emerging applications from porous properties,<sup>[14,16–19]</sup> such as catalysis,<sup>[20,21]</sup> gas adsorption,<sup>[14,22]</sup> and electric double-layer capacitors (EDLCs).<sup>[23]</sup> The advantages for the use of these functional polymeric frameworks are non-toxicity, absence of expensive rare earth elements, high stability of the frameworks, and, most importantly, the possibility to change the electronic properties by changing the structure.<sup>[16]</sup> These features make this class of polymers an interesting candidate for the electrode material in rechargeable electrical energy storage devices.

Inspired by these considerations, we investigated amorphous covalent triazine-based frameworks (ACTFs) synthesized from *p*-dicyanobenzene, ACTF-1. It provides a high specific capacity and power, which are delivered by a unique energy storage mechanism using both p- and n-doped states for the cathode, and consequently shows a capacity-like bipolar redox reaction with a linear transition from each doped state in the energy storing process, a large working potential because of the high stability of C–N bonds in the framework,<sup>[14]</sup> rapid ion transport by the electrolyte-filled porous network,<sup>[12]</sup> and a large electrode surface area. The combined characteristics of a porous polymeric framework cathode that consists of triazine rings result in a remarkably high specific energy and high specific power.

The covalent triazine-based frameworks were synthesized in both an amorphous (ACTF-1) and a crystalline state (Supporting Information, Figure S1).<sup>[15]</sup> The results of the nitrogen physisorption experiments and the FTIR spectroscopy measurements of CTFs and other synthesized porous polymeric frameworks confirm the high specific surface area and high purity of the materials (Supporting Information, Figures S2, S3). The porous morphology of ACTF-1 is confirmed by high-resolution transmission electron microscopy (HRTEM) observations and the pore-size distribution (Supporting Information, Figure S4). Cyclic voltammetry (CV) measurements were carried out to investigate the fundamental electrochemical properties of the porous polymeric

[\*] K. Sakaushi, Prof. Dr. J. Eckert

Institute for Complex Materials, IFW Dresden  
Helmholtzstrasse 20, 01069 Dresden (Germany)  
E-mail: k.sakaushi@ifw-dresden.de

K. Sakaushi, G. Nickerl, F. M. Wisser, Prof. Dr. S. Kaskel  
Department of Inorganic Chemistry, TU Dresden (Germany)

Prof. Dr. J. Eckert  
Institute of Materials Science, TU Dresden (Germany)

Dr. D. Nishio-Hamane  
Institute for Solid State Physics (ISSP), The University of Tokyo  
(Japan)

Dr. E. Hosono, Prof. Dr. H. Zhou  
Energy Technology Research Institute, National Institute of  
Advanced Industrial Science and Technology (AIST) (Japan)  
E-mail: hs.zhou@aist.go.jp

[\*\*] We are grateful to Prof. Dr. T. Kudo (AIST/Univ. Tokyo) for his valuable comments. We thank for Dr. S. Pauly, Dr. P. Dunne, and members of their laboratories. This work was partially performed using facilities of ISSP (Univ. Tokyo). K.S. is supported by DAAD under the grant number of A/09/74990.



Supporting information for this article is available on the WWW under <http://dx.doi.org/10.1002/anie.201202476>.

electrodes by using 1M LiPF<sub>6</sub> in ethylene carbonate/dimethyl carbonate (1:1) as the electrolyte. ACTF-1 shows a significant improved electrochemical reaction compared to crystalline CTF-1 (Figure 1a; for details, see the Supporting Information). The performance of the benzene-based polymeric framework (organic frameworks by cyclotrimerization

maintain electroneutrality during their oxidation and reduction.<sup>[25,26]</sup>

A CV measurement at a very slow scan rate of 0.1 mV s<sup>-1</sup> shows several redox peaks in both p- and n-doping regions (Figure 2a). These peaks are confirmed by open-circuit voltage (OCV) curves (Figure 2b,c; Supporting Information,

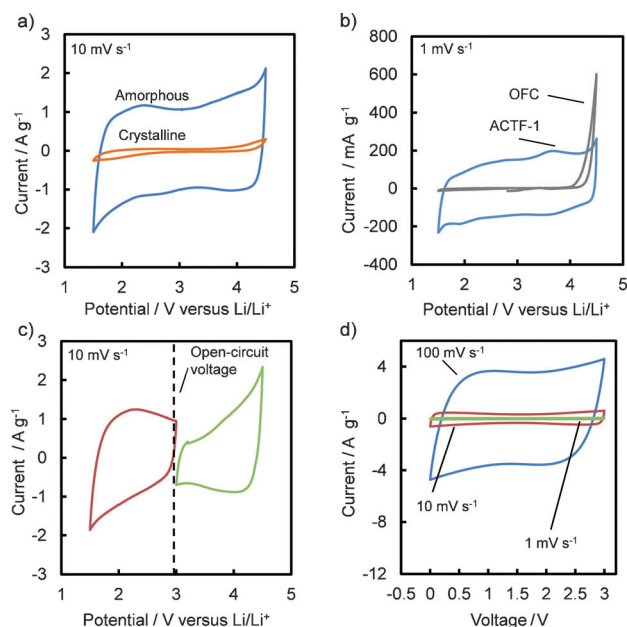


**Figure 1.** a) Comparison of cyclic voltammetry data of a) ACTF-1 and CTF-1 and b) ACTF-1 and OFC. c) Cyclic voltammogram data for an ACTF-1 electrode obtained above and below the open-circuit voltage (3 V vs. Li/Li<sup>+</sup>). d) Cyclic voltammogram data for a polymer/polymer cell. The scan speed applied ranges from 1.0 mV s<sup>-1</sup> to 100 mV s<sup>-1</sup>.

(OFC); Ref. [22]) indicates that the triazine rings are involved in the electrochemical reaction of ACTF-1 and responsible for the stability in the potential range of 1.5–4.5 V versus Li/Li<sup>+</sup> because the main difference between the two polymeric frameworks is the presence of triazine rings (Figure 1b). Moreover, ordered CTF-1 and OFC show low specific capacitances despite their high surface areas (Supporting Information, Table S1). This result indicates that energy storage mechanism of ACTF-1 is different from EDLCs because the electrochemical property of EDLCs is dependent on the specific surface area of porous materials. The cyclic voltammogram of ACTF-1 electrodes below and above the open-circuit voltage of 3 V versus Li/Li<sup>+</sup> (Figure 1c) suggests that ACTF-1 has a reduced (n-doped) state below 3 V versus Li/Li<sup>+</sup> and an oxidized (p-doped) state above 3 V versus Li/Li<sup>+</sup>. CV measurements were carried out at various scan rates for a symmetrical polymer/polymer cell using ACTF-1 as a cathode and an anode to check the bipolarity of ACTF-1 (Figure 1d).<sup>[24]</sup> The current at 2.5 V was found to increase linearly with scan rate (Supporting Information, Figure S5), indicating a surface-limited redox process.<sup>[11]</sup> The existence of a reduced and oxidized state is indispensable if this material is to be used as the electrode in a rechargeable energy storage device. Such polymer electrodes take up or give off ions to

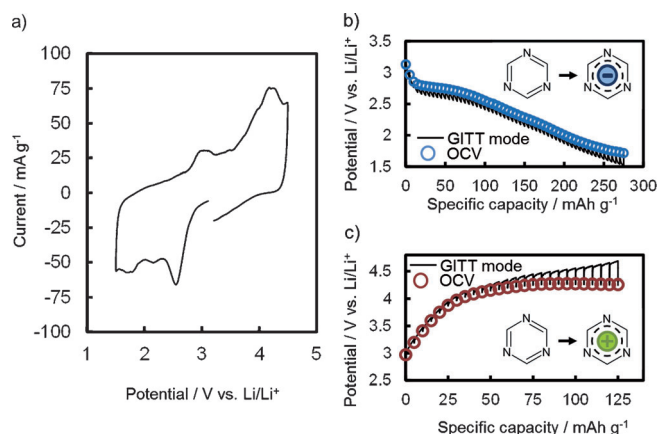


**Figure 2.** a) Cyclic voltammetry data of ACTF-1 at 0.1 mV s<sup>-1</sup>, b) OCV curve from initial OCV to the n-doping region (1.5 V vs. Li/Li<sup>+</sup>), and c) OCV curve from initial OCV to the p-doping region (4.7 V vs. Li/Li<sup>+</sup>). Solid lines show the voltage change during GITT experiments.

Figure S6), which were taken by the galvanostatic intermittent titration technique (GITT). Both OCV curves were measured from initial OCV (3 V vs. Li/Li<sup>+</sup>) of ACTF-1 to the n- or p-doping region, respectively, as only the information about the n- or p-doping process is desired. Clear redox peaks at 2.8 and 4.2 V versus Li/Li<sup>+</sup> were observed in CV data (Figure 2a). These redox peaks were confirmed by the plateaus in the OCV curves: the plateau for n-doping process is at 2.8 V versus Li/Li<sup>+</sup> in Figure 2b, and p-doping is at 4.2 V versus Li/Li<sup>+</sup> in Figure 2c (for more details, see the Supporting Information).

In situ electrochemical impedance spectroscopy (EIS) measurements were performed to study the electrochemical energy storage mechanism of ACTF-1 in more detail. A frequency range from 10 mHz to 10 kHz with an amplitude of 5 mV was applied for ACTF-1 in the p-doping and n-doping region, respectively (Supporting Information, Figure S7 and Experimental Section). The Nyquist plots in both the n-doping and p-doping region show a semicircle, which suggests the existence of charge transfer at the ACTF-1/electrolyte interface, and Warburg impedance tilt angles of almost 45° show a typical redox electrochemical reaction (Supporting Information, Figure S7).<sup>[27,28]</sup> PF<sub>6</sub><sup>-</sup>, which was electrochemically doped in ACTF-1, was detected by FTIR and Raman spectroscopy measurements (Supporting Information, Figure S8). Those results suggest that the energy storage mechanism of ACTF-1 is processed by both p- and n-doping mechanism. Therefore, it is suggested that the energy storage principle of ACTF-1 is based on a bipolar Faradaic reaction.

From our investigations, we propose a possible electrochemical reaction mechanism for the ACTF-1 (Figure 3; for

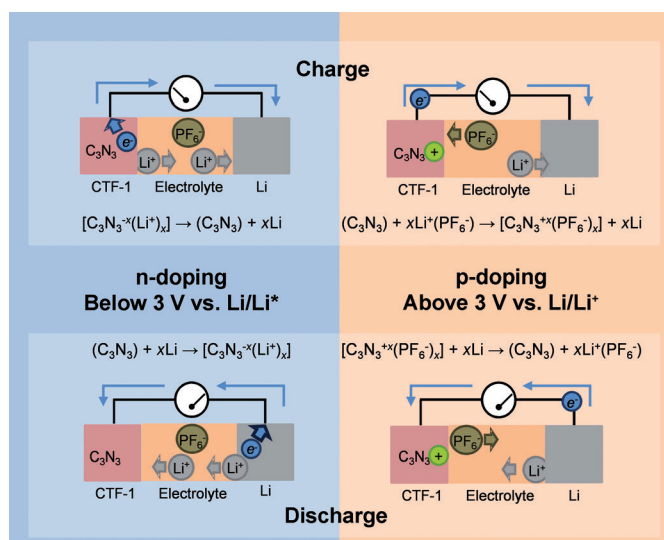
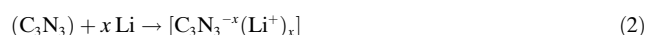
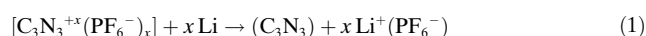


**Figure 3.** Electrical energy storage mechanism of ACTF-1. See the Supporting Information for details.

details, see the Supporting Information, discussion and Scheme S1). The triazine ring,  $C_3N_3$ , in the potential range below 3 V versus  $Li/Li^+$  (initial open-circuit voltage) can be reduced and oxidized according to  $(C_3N_3) + xe^- \rightleftharpoons C_3N_3^{-x}$ . In the potential range above 3 V versus  $Li/Li^+$ , using  $LiPF_6$  as a Li salt in the electrolyte, the redox reaction of  $C_3N_3$  involving with anion ( $PF_6^-$ ) is expected to occur according to  $(C_3N_3) + xPF_6^- \rightleftharpoons [C_3N_3^{+x}(PF_6^-)_x] + xe^-$ .<sup>[25,26]</sup> Considering these two reactions with the reaction at the anode ( $Li$  metal):  $xLi \rightleftharpoons xLi^+ + xe^-$ , the charge and the discharge processes of  $C_3N_3$  occur in two continuous linear redox reactions. For example, for the discharge process from 4.5 to 1.5 V versus  $Li/Li^+$ , the first reaction (4.5–3.0 V vs.  $Li/Li^+$ ) can be described by Equation (1). The continuous and linear transition from p-doped state (oxidized state) to the n-doped state (reduced state) leads to Equation (2) below 3.0 V versus  $Li/Li^+$ .  $PF_6^-$  is supplied from the electrolyte, but  $Li^+$  is supplied from the anode.



This energy storage system is different from current rechargeable lithium batteries using the intercalation mechanism and it is different from organic batteries, including all-organic batteries, which use bipolar redox active polymers for a p-dopable polymer cathode and n-dopable polymer anode.<sup>[1–13,23,25,26,29–31]</sup> The neutral state of the triazine rings bridges its oxidized state [Eq. (1)] and reduced state [Eq. (2)] linearly and continuously by the continuous linear bipolar redox mechanism (Figure 3). This unique mechanism for ACTF-1 delivers the high-performance electrochemical properties.

The electrical energy storage characteristics of ACTF-1 electrodes were measured in two working potentials of 1.5–4.5 V versus  $Li/Li^+$  and 1.0–5.0 V versus  $Li/Li^+$ . The charge–

discharge profiles at various current densities from  $0.05 \text{ A g}^{-1}$  to  $20 \text{ A g}^{-1}$  in the working potential of 1.5–4.5 V versus  $Li/Li^+$  are shown in Figure 4a. At a constant current density of  $0.05 \text{ A g}^{-1}$ , the ACTF-1 electrode shows a specific capacity of about  $160 \text{ mA h g}^{-1}$  based on the mass of ACTF-1 with a sloping voltage profile. Even for the remarkably high current density of  $20 \text{ A g}^{-1}$ , ACTF-1 can provide a specific capacity of  $60 \text{ mA h g}^{-1}$ . This is equivalent to a 125C rate, if we assume  $160 \text{ mA h g}^{-1}$  as the specific capacity of ACTF-1 in the working potential of 1.5–4.5 V versus  $Li/Li^+$ . The rate of  $nC$  corresponds to a full discharge in  $1/n$  h. The cycle performance of ACTF-1 electrodes was checked for at various current densities (Figure 4b), revealing quite a good cycle stability. Even under rather harsh conditions (25 cycles at different current densities from  $0.1 \text{ A g}^{-1}$  to  $20 \text{ A g}^{-1}$  without relaxation between the cycles), ACTF-1 reproduces the stable

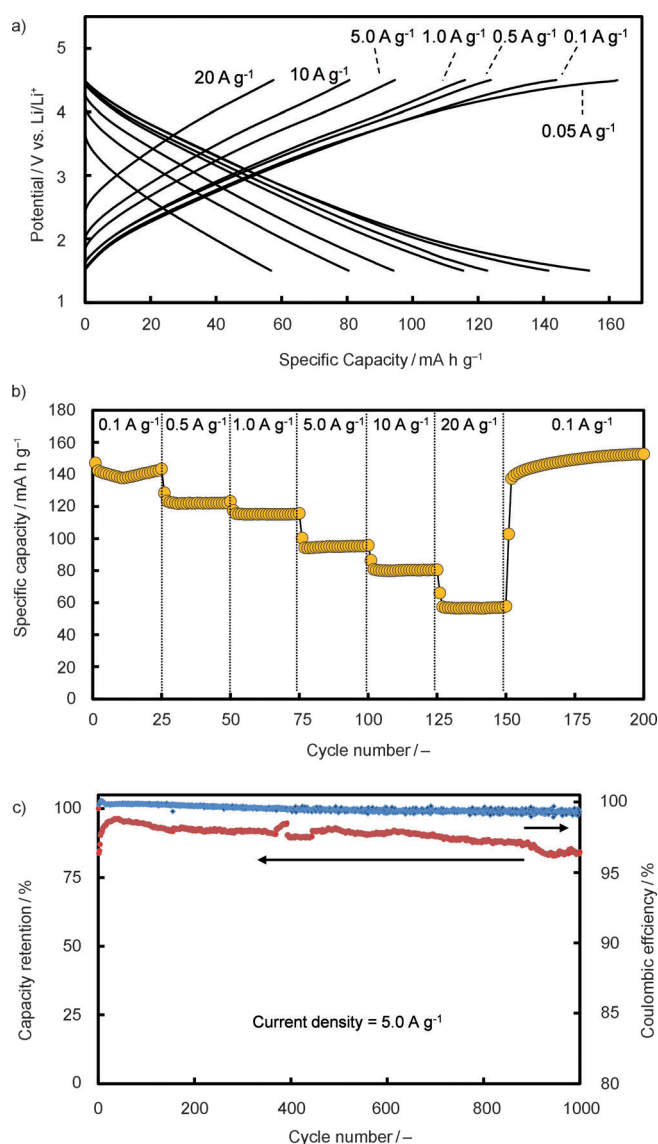


**Figure 4.** a) Charge–discharge profiles of ACTF-1 at various current densities. b) Cycle performance at various current densities. c) Cycle performance of ACTF-1 up to 1000 cycles with a current density of  $5.0 \text{ A g}^{-1}$ .

specific capacity of about  $150 \text{ mAh g}^{-1}$  at  $0.1 \text{ A g}^{-1}$ , thus retaining the same specific capacity as in the first 25 cycles at  $0.1 \text{ A g}^{-1}$ . Moreover, ACTF-1 electrodes can be tested up to 1000 cycles with 84 % capacity retention at the high current density of  $5.0 \text{ A g}^{-1}$  (Figure 4c).

The cyclic voltammogram for ACTF-1 in the potential range of 1.0–5.0 versus  $\text{Li/Li}^+$  is shown in the Supporting Information, Figure S9a. At this working potential, the ACTF-1 electrode shows a high specific capacity of  $542 \text{ mAh g}^{-1}$  at a constant current density of  $0.05 \text{ A g}^{-1}$ , and  $164 \text{ mAh g}^{-1}$  at a constant current density of  $5.0 \text{ A g}^{-1}$  (Supporting Information, Figure S9b). After cycling up to 50 times at  $5.0 \text{ A g}^{-1}$ , a capacity retention of 70 % was observed (Supporting Information, Figure S9c). ACTF-1 electrodes show a high specific energy of  $340 \text{ Wh kg}^{-1}$  combined with a high specific power of  $50085 \text{ W kg}^{-1}$  based on the mass of ACTF-1 in the working potential of 1.5–4.5 V versus  $\text{Li/Li}^+$ . At the working potential of 1.0–5.0 V versus  $\text{Li/Li}^+$ , ACTF-1 can deliver a remarkably high specific energy of  $1084 \text{ Wh kg}^{-1}$  and a specific power of  $13238 \text{ W kg}^{-1}$  based on the mass of ACTF-1 (for the calculation of specific energy  $E$  ( $\text{Wh kg}^{-1}$ ) and specific power  $P$  ( $\text{W kg}^{-1}$ ), see the Supporting Information, Experimental Section and Figure S10). These results reveal the high electrochemical performances of ACTF-1 compare well with typical specific energy and specific power of lithium-ion battery materials, ranged from about  $500 \text{ Wh kg}^{-1}$  (Ref. [11]) and  $500\text{--}2000 \text{ W kg}^{-1}$  (Ref. [10]).

Assuming that the ACTF-1 constitutes 35 % of the total mass of active materials in a full cell, this full cell will produce a high specific energy of  $119 \text{ Wh kg}_{\text{cell}}^{-1}$  while showing a high specific power of  $17529 \text{ W kg}_{\text{cell}}^{-1}$  at a working potential of 1.5–4.5 V versus  $\text{Li/Li}^+$  (Figure 5, red). In the case of a working potential of 1.0–5.0 V versus  $\text{Li/Li}^+$  (Figure 5, blue), the specific energy of ACTF-1/Li cells will reach  $379 \text{ Wh kg}_{\text{cell}}^{-1}$  with a specific power of  $4633 \text{ W kg}_{\text{cell}}^{-1}$ , which is comparable to the specific energy of fuel cells and the specific power of electrochemical supercapacitors.<sup>[3]</sup>

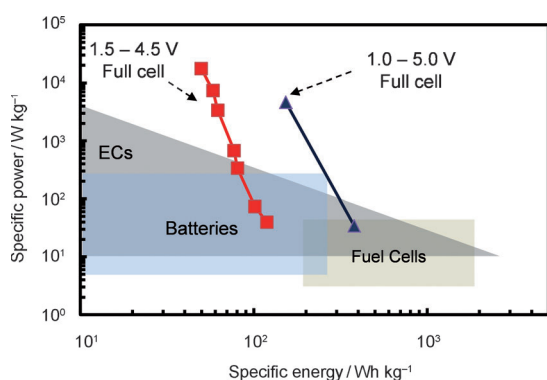


**Figure 5.** Comparison of specific power and specific energy (Ragone plot) of ACTF-1/Li cells and various electrical energy storage devices. ACTF-1/Li full cells at a working potential of 1.5–4.5 V versus  $\text{Li/Li}^+$  are indicated by red, and at a working potential of 1.0–5.0 V versus  $\text{Li/Li}^+$  by blue. ECs = electrochemical capacitors. A full cell is estimated based on the assumption that the ACTF-1 constitutes 35 % of the total mass of the active materials in a cell.

In summary, our findings suggest that ACTF-1 is a promising metal-free porous polymeric framework with a new energy storage principle, which uses both p-doping and n-doping as a cathode material. Based on this energy storage concept, we have demonstrated an unusually high specific energy and specific power. The lithium organic system based on ACTFs reaches a performance comparable to other possible next-generation energy storage systems, such as lithium–air and lithium–sulfur systems. The ability to further increase their specific power and energy could be possible due to the wide variety of different functional frameworks and starting monomers. This would significantly extend the possibilities of electrical energy storage, while avoiding the use of toxic transition metals or rare-earth elements in today's high-performance batteries.

Received: March 30, 2012

Published online: June 21, 2012

Please note: Minor changes have been made to this manuscript since its publication in *Angewandte Chemie* Early View. The Editor.

**Keywords:** amorphous materials · bipolarity · energy storage · polymeric frameworks · porous materials

- [1] M. Armand, J. M. Tarascon, *Nature* **2008**, *451*, 652–657.
- [2] A. S. Aricò, P. G. Bruce, B. Scrosati, J. M. Tarascon, W. Van Schalkwijk, *Nat. Mater.* **2005**, *4*, 366–377.
- [3] M. S. Whittingham, *MRS Bull.* **2008**, *33*, 411–419.
- [4] P. Simon, Y. Gogotsi, *Nat. Mater.* **2008**, *7*, 845–854.
- [5] J. M. Tarascon, *Philos. Trans. R. Soc. London Ser. A* **2010**, *368*, 3227–3241.
- [6] Y. G. Wang, H. Li, P. He, E. Hosono, H. S. Zhou, *Nanoscale* **2010**, *2*, 1294–1305.
- [7] Y. G. Wang, P. He, H. S. Zhou, *Energy Environ. Sci.* **2011**, *4*, 4994–4999.
- [8] K. S. Kang, Y. S. Meng, J. Breger, C. P. Grey, G. Ceder, *Science* **2006**, *311*, 977–980.
- [9] Y. G. Wang, Y. R. Wang, E. Hosono, K. X. Wang, H. S. Zhou, *Angew. Chem.* **2008**, *120*, 7571–7575; *Angew. Chem. Int. Ed.* **2008**, *47*, 7461–7465.
- [10] B. Kang, G. Ceder, *Nature* **2009**, *458*, 190–193.
- [11] S. W. Lee, N. Yabuuchi, B. M. Gallant, S. Chen, B. S. Kim, P. T. Hammond, Y. Shao-Horn, *Nat. Nanotechnol.* **2010**, *5*, 531–537.
- [12] H. Zhang, X. Yu, P. V. Braun, *Nat. Nanotechnol.* **2011**, *6*, 277–281.
- [13] T. Ogasawara, A. Débart, M. Holzapfel, P. Novák, P. G. Bruce, *J. Am. Chem. Soc.* **2006**, *128*, 1390–1393.
- [14] A. P. Côté, A. I. Benin, N. W. Ochwig, M. O'Keefe, A. J. Matzger, O. M. Yaghi, *Science* **2005**, *310*, 1166–1170.
- [15] P. Kuhn, M. Antonietti, A. Thomas, *Angew. Chem.* **2008**, *120*, 3499–3502; *Angew. Chem. Int. Ed.* **2008**, *47*, 3450–3453.
- [16] A. I. Cooper, *Adv. Mater.* **2009**, *21*, 1291–1295.
- [17] J. X. Jiang, A. I. Cooper, *Top. Curr. Chem.* **2010**, *293*, 1–33.
- [18] A. Thomas, *Angew. Chem.* **2010**, *122*, 8506–8523; *Angew. Chem. Int. Ed.* **2010**, *49*, 8328–8344.
- [19] A. Thomas, P. Kuhn, J. Weber, M. M. Titirici, M. Antonietti, *Macromol. Rapid Commun.* **2009**, *30*, 221–236.
- [20] X. C. Wang, M. Maeda, A. Thomas, K. Takanabe, G. Xin, J. M. Carlsson, K. Domen, M. Antonietti, *Nat. Mater.* **2009**, *8*, 76–80.
- [21] R. Palkovits, M. Antonietti, P. Kuhn, A. Thomas, F. Schüth, *Angew. Chem.* **2009**, *121*, 7042–7045; *Angew. Chem. Int. Ed.* **2009**, *48*, 6909–6912.



- [22] M. Rose, N. Klein, I. Senkovska, C. Schrage, P. Wollmann, W. Böhlmann, B. Böhringer, S. Fichtner, S. Kaskel, *J. Mater. Chem.* **2011**, *21*, 711–716.
- [23] Y. Kou, Y. Xu, Z. Guo, D. Jiang, *Angew. Chem.* **2011**, *123*, 8912–8916; *Angew. Chem. Int. Ed.* **2011**, *50*, 8753–8757.
- [24] K. Oyaizu, T. Sukegawa, H. Nishide, *Chem. Lett.* **2011**, *40*, 184–185.
- [25] P. J. Nigrey, D. MacInnes, D. P. Nairns, A. G. MacDiarmid, A. J. Heeger, *J. Electrochem. Soc.* **1981**, *128*, 1651–1654.
- [26] P. Novák, K. Müller, S. V. Santhanam, O. Hass, *Chem. Rev.* **1997**, *97*, 207–281.
- [27] P. G. Bruce, M. Y. Saidi, *J. Electroanal. Chem.* **1992**, *332*, 93–105.
- [28] Y. Mizuno, M. Okubo, D. Asakura, T. Saito, E. Hosono, Y. Saito, K. Oh-ishi, T. Kudo, H. S. Zhou, *Electrochim. Acta* **2012**, *63*, 139–145.
- [29] H. Nishide, T. Suga, *Electrochem. Soc. Interface* **2005**, *15*, 32.
- [30] H. Chen, M. Armand, G. Demailly, F. Dolhem, P. Poizot, J. M. Tarascon, *ChemSusChem* **2008**, *1*, 348–355.
- [31] T. Suga, H. Ohshiro, S. Sugita, K. Oyaizu, H. Nishide, *Adv. Mater.* **2011**, *23*, 1627–1630.